Journal Pre-proof

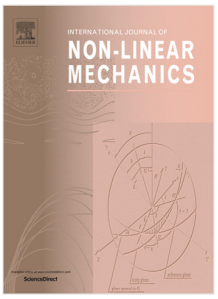

Advancing contact of a 2D elastic curved beam indented by a rigid pin with clearance

E. Radi, A. Strozzi

PII: S0020-7462(22)00283-9
DOI: https://doi.org/10.1016/j.ijnonlinmec.2022.104313
Reference: NLM 104313

To appear in: *International Journal of Non-Linear Mechanics*

Received date : 5 November 2022
Revised date : 24 November 2022
Accepted date : 25 November 2022

Please cite this article as: E. Radi and A. Strozzi, Advancing contact of a 2D elastic curved beam indented by a rigid pin with clearance, *International Journal of Non-Linear Mechanics* (2022), doi: https://doi.org/10.1016/j.ijnonlinmec.2022.104313.

ADVANCING CONTACT OF A 2D ELASTIC CURVED BEAM INDENTED BY A RIGID PIN WITH CLEARANCE

E. Radi[1], A. Strozzi[2]

[1]*Dipartimento di Scienze e Metodi dell'Ingegneria, Università di Modena e Reggio Emilia, Via G. Amendola 2, I-42122 Reggio Emilia, Italy. Email: enrico.radi@unimore.it*

[2]*Dipartimento di Ingegneria "Enzo Ferrari", Università di Modena e Reggio Emilia, Via Vivarelli, 10, I-41125 Modena, Italy. Email: antonio.strozzi@unimore.it*

Abstract. A two-dimensional analytical solution is presented for stresses and displacements in an elastic curved beam forming an incomplete ring in frictionless and unbonded contact with a rigid pin loaded by a point force and in the presence of clearance. The circular beam is modelled as an incomplete elastic thick ring, constrained at both ends and in a plane stress state. The stress and displacement fields within the beam are derived from a biharmonic Airy stress function, according to the Michell solution in polar coordinates. The mixed boundary value problem is reduced to a set of dual series equations and then to a non-homogeneous linear system of infinite equations, which is then solved by truncation. The non-linear relations between the applied load and the contact angle or the pressure distribution are obtained by using an inverse method. The analytical results are compared with finite element predictions for a pin-lug connection and a reasonable agreement is observed for several typical geometries. The peaks of contact pressure and von Mises equivalent stress and their location within the curved beam are evidenced.

Keywords: Biharmonic equation, Curved beam, Advancing contact, Inverse method, Clearance, Dual series.

1. Introduction

Contact problems for a loaded pin connection with clearance are frequently met in mechanical and structural engineering, because a small amount of clearance is necessarily required for improving the rotational performance of the circular pin. On the other side, clearance is also responsible for vibration, noise and wear in mechanical connections, and thus its amount must be kept at the minimum allowable level. Due to their complexity arising from the progressive increase of the unknown contact region with the loading, which is responsible of the non-linear response though the material behavior is linear elastic, these problems are usually treated by advanced numerical techniques and only few analytical studies are available in the literature. Most of them concern the problem of the advancing contact of a circular pin in a hole in an infinite elastic medium [1-6], and

only a few of them deal with the case of pin-lug connections [7-9]. The problem still attracts the interest of the researchers, due to the progressive feature of the pin-lug contact, and to the appearance of considerable pressure bumps at the contact extremities, which may increase wear failure of the connection. An interesting aspect for mechanical engineers is the value of the load that produces a contact arc close to π. For loads beyond this limit, the contact problem becomes virtually linear, and the contact pressure becomes essentially proportional to the applied load, so that the stresses may be computed by a standard finite element method (FEM). In [10] a load factor is proposed that, although approximately, is connected to the contact angular extent. This load factor summarizes the effect of the load, the Young's modulus, the initial clearance, and the lug geometry.
Additional studies regard the possibility of interpreting the point loads at the pin-lug contact extremities, appearing if the lug is described by the 1D beam theory beam, as pressure bumps of finite value. This interpretation would permit the lug stress field to be more realistically estimated. This approach is discussed in [11], and it relies on the Hertzian theory and Saint Venant hypothesis. Another aspect worth of interest is the effect of an oblique load acting on the pin, see [12, 13]. An interesting point is the location of the lug maximum equivalent stress. For low loads, the maximum stress occurs at the contact center. When the load is increased, the maximum stress moves abruptly laterally, at the sides of the bore. It is relevant to know for which load factor this shift of the maximum stress occurs. The above aspects describing the pin-lug mechanical response fully justify the attention of the researchers towards pinned connections and related contact problems.
Pinned connections provide a mechanical link between lugs without precluding relative rotations. The determination of the contact angular width in terms of the applied load and of the initial clearance is a fundamental aspect in the understanding of the mechanical response of the pin-lug connections. The most employed model of this connection adopts a rigid, solid pin in contact with a lug described as an incomplete ring of constant radial width, clamped at both extremities. More precisely, two models of the incomplete ring are generally favored in the pertinent literature, namely a) a ring modelled as a curved beam according to the one-dimensional (1D) beam theory, and b) a ring mimicked as a two-dimensional (2D) annulus in terms of the 2D theory of elasticity.

To contain the mathematical difficulties, a purely flexural 1D beam model is often preferred, e. g. [10]. However, this model assumes transversal inextensibility of the beam and thus predicts underestimated contact lengths usually. Moreover, it demands that the contact reaction between the pin and the lug be described by a constant pressure profile along the pin-lug contact arc for the lug to exhibit a constant curvature, endowed with unrealistic radial concentrated forces directed outwards, see [14]. These forces appear in order to avoid any unphysical compenetration between the pin contour and the inner border of the lug portion detached from the pin. The presence of

physically unrealistic concentrated forces still delivers a realistic mathematical connection between the pin-lug contact extent on one side, and the applied load and the initial clearance on the other side. Conversely, the presence of point forces precludes the possibility of predicting reliable stresses within the lug.

In the present work, a simplified geometry is adopted for the lug, modelled as an incomplete 2D elastic ring of constant radial width clamped at its extremities and indented by a rigid pin, in the presence of initial clearance. A Michell-type series representation is considered for the stress and displacement fields, according to the 2D theory of linear and isotropic elasticity, and a fully analytical approach based on the solution of a dual trigonometric series is adopted. This model is considerably more complex than its 1D curved beam counterpart, but it can consider the transversal deformability of the indented beam and it avoids the outcome of point forces at the pin-lug contact extremities. In fact, the 2D model produces realistic pressure bumps at the contact extremities, as confirmed by photoelastic studies [12]. As a counterpart, the adopted 2D model does not simulate exactly the geometry of the lug, whose thickness actually increases at the transition between the lug curved shape and the lug shank. To simulate the presence of the lug shank, the angular extent of the 2D curved beam is extended beyond π, based on a matching procedure with the predictions of a FEM analysis.

The analytical approach adopted here is suggested by the studies [15-17], which investigated the plane contact problems of a circular inclusion embedded in an infinite elastic medium or in a thick-walled tube, as well as by the work [18], which addressed the problem of the indentation of an incomplete elastic ring by a rigid flat surface. By using a modified Michell solution for a biharmonic stress function in polar coordinates, these authors reduced the mixed boundary value problems with circular boundaries arising in the study of contact problems in 2D elasticity to dual trigonometric series and then to integral equations of the Fredholm type. Here, we transform the dual series equations to a non-homogeneous linear system of infinite equations, which is then solved by truncation. Due to the progressive and nonlinear increase of the unknown contact length between pin and lug with the applied load, this procedure requires an inverse method of solution. Namely, we impose a specified angular contact extent and then seek to determine the magnitude of the load causing that contact angle. By finding a number of these linear elastic solutions for increasing contact lengths, the non-linear relationship between the contact angle and a loading parameter proportional to the ratio between the load magnitude and the clearance is then obtained.

Finally, the analytical results in terms of the contact angular extent are compared with the FEM predictions for a pin-lug connection and a reasonable agreement is observed for a large range of aspect ratios, after proper calibration of the curved beam angular extent.

2. Problem formulation

We consider the plane problem of an elastic circular thick beam in Fig. 1 with an angular extent of 2β, whose inner and outer radii are denoted by r_i and r_o, respectively, indented by a rigid pin with radial clearance $\delta = r_i - r_p$, where r_p is the pin radius, under plane stress loading conditions. Due to the effect of clearance, the contact problem is progressive, and the contact length between the two components increases with the load P applied to the pin. Therefore, a special procedure based on the inverse method of solution is required to evaluate the contact extent. The problem aims to simulate the loading condition of a typical pin-lug connection.

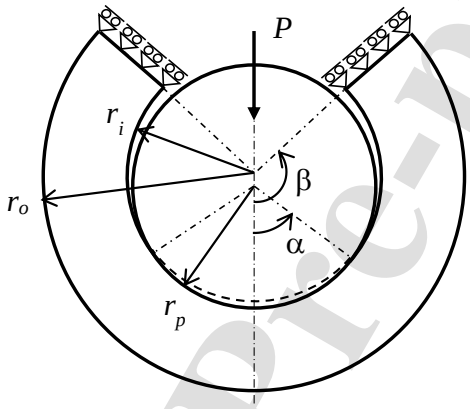

Figure 1. 2D Curved beam indented by a rigid pin.

Reference is made to a polar coordinate system $(0, r, \theta)$ whose origin lays at the center of the circular curved beam and the polar axis $\theta = 0$ coincides with the direction of the load P applied to the rigid pin (Fig. 1). The boundary conditions must require that the lower outer surface of the beam is stress free, namely

$$\sigma_{rr} = \sigma_{r\theta} = 0, \qquad \text{for} \quad 0 \le |\theta| \le \beta, \quad r = r_o. \tag{2.1}$$

whereas the upper inner surface is subject to mixed load and displacement boundary conditions due to the frictionless unbonded contact with the rigid pin, namely

$$\begin{aligned} &\sigma_{r\theta} = 0, \qquad \text{for} \quad 0 \le |\theta| \le \beta, \quad r = r_i, \\ &\sigma_{rr} = 0, \qquad \text{for} \quad \alpha \le |\theta| \le \beta, \quad r = r_i, \\ &u_r = v \cos\theta - \delta(1 - \cos\theta), \qquad \text{for} \quad 0 \le |\theta| \le \alpha, \quad r = r_i, \end{aligned} \tag{2.2}$$

where δ is the radial clearance and v_0 denotes an unknown rigid body motion of the pin along the loading direction. The last contact condition on the radial displacement along the contact zone in the clearance case was obtained in [19, 20] for the almost conforming contact problem between a

cylindrical pin and a hole in a plate, namely for $\delta << r_i$. Finally, the circumferential displacements and shear tractions are assumed to vanish at the beam ends, namely

$$u_\theta = \sigma_{r\theta} = 0, \qquad \text{for} \quad |\theta| = \beta, \quad r_i \le r \le r_o. \tag{2.3}$$

Since the loading condition is symmetric with respect to the vertical axis ($\theta = 0$), then following [18] and [21] we take the following cylindrical components of the stress, which are obtained by means of a biharmonic Airy stress function containing only even terms in θ, according to the Michell solution (for analytical details see Appendix A)

$$\begin{aligned}
\frac{\sigma_{rr}(r,\theta)}{2\mu} &= \frac{\delta}{r_o}\left\{-\sum_{n=1}^{\infty}\cos m\theta\left[(m-1)m\,a_n\left(\frac{r}{r_o}\right)^{m-2}+(m-2)(m+1)\,b_n\left(\frac{r}{r_o}\right)^{m}+(m+1)\,c_n\left(\frac{r}{r_o}\right)^{-m-2}+(m-1)(m+2)\,d_n\left(\frac{r}{r_o}\right)^{-m}\right]\right. \\
&\quad \left. +2a_0+\frac{b_o}{r^2}\right\}, \\
\frac{\sigma_{\theta\theta}(r,\theta)}{2\mu} &= \frac{\delta}{r_o}\left\{\sum_{n=1}^{\infty}\cos m\theta\left[(m-1)m\,a_n\left(\frac{r}{r_o}\right)^{m-2}+(m+2)(m+1)\,b_n\left(\frac{r}{r_o}\right)^{m}+m(m+1)\,c_n\left(\frac{r}{r_o}\right)^{-m-2}+(m-1)(m-2)\,d_n\left(\frac{r}{r_o}\right)^{-m}\right]\right. \\
&\quad \left. +2a_0-\frac{b_o}{r^2}\right\}, \\
\frac{\sigma_{r\theta}(r,\theta)}{2\mu} &= \frac{\delta}{r_o}\sum_{n=1}^{\infty}\sin m\theta\left[(m-1)m\,a_n\left(\frac{r}{r_o}\right)^{m-2}+m(m+1)\,b_n\left(\frac{r}{r_o}\right)^{m}-m(m+1)\,c_n\left(\frac{r}{r_o}\right)^{-m-2}-m(m-1)\,d_n\left(\frac{r}{r_o}\right)^{-m}\right],
\end{aligned} \tag{2.4}$$

where $m = n\pi/\beta$, μ is the elastic shear modulus of the curved beam, and a_0, b_0, a_n, b_n, c_n, and d_n are arbitrary constants to be determined from the boundary conditions. The corresponding displacement fields are [21]:

$$\begin{aligned}
\frac{u_r}{\delta} &= -\sum_{n=1}^{\infty}\cos m\theta\left[m\,a_n\left(\frac{r}{r_o}\right)^{m-1}+(m+1-\kappa)\,b_n\left(\frac{r}{r_o}\right)^{m+1}-m\,c_n\left(\frac{r}{r_o}\right)^{-m-1}-(m-1+\kappa)\,d_n\left(\frac{r}{r_o}\right)^{-m+1}\right] \\
&\quad -\frac{b_o}{r}-\frac{r}{r_o}(1-\kappa)\,a_o, \\
\frac{u_\theta}{\delta} &= \sum_{n=1}^{\infty}\sin m\theta\left[m\,a_n\left(\frac{r}{r_o}\right)^{m-1}+(m+1+\kappa)\,b_n\left(\frac{r}{r_o}\right)^{m+1}+m\,c_n\left(\frac{r}{r_o}\right)^{-m-1}+(m-1-\kappa)\,d_n\left(\frac{r}{r_o}\right)^{-m+1}\right],
\end{aligned} \tag{2.5}$$

where κ is the Kolosov's constant [21], namely

$$\kappa = \begin{cases} 3-4\nu & \text{for plane strain,} \\ \dfrac{3-\nu}{1+\nu} & \text{for plane stress,} \end{cases} \tag{2.6}$$

and ν is the Poisson's ratio of the material. The boundary conditions (2.1) and $(2.2)_1$ then provides the constants b_n, c_n, and d_n in terms of a_n, for n = 0, 1, 2,.., namely

$$\begin{aligned}
b_0 &= -2r_o\, a_0,\\
b_n &= \frac{(m-1)\left(1-\rho^{2m}-m\rho^2+m\right)}{(m+1)\left(\rho^{2m+2}+m\rho^2-m-\rho^2\right)}\, a_n,\\
c_n &= \frac{(m-1)\left(m\rho^{2m+2}+\rho^{2m+2}-m\rho^{2m}-\rho^2\right)}{(m+1)\left(\rho^{2m+2}+m\rho^2-m-\rho^2\right)}\, a_n,\\
d_n &= \frac{m\rho^{2m}-\rho^{2m}-m\rho^{2m+2}+1}{\rho^{2m+2}+m\rho^2-m-\rho^2}\, a_n,
\end{aligned} \tag{2.7}$$

where $\rho = r_i/r_o < 1$ denotes the aspect ratio of the curved beam. The remaining boundary conditions on the upper beam surface $(2.2)_{2,3}$ then yield a set of dual trigonometric series

$$\frac{A_0}{2}+\sum_{n=1}^{\infty}A_n\cos\frac{n\pi}{\beta}\theta=0, \qquad \text{for} \quad \alpha\le|\theta|\le\beta, \tag{2.8}$$

$$\frac{A_0}{2}\frac{\rho^2}{1-\rho^2}\left(\frac{2}{\rho}-\rho+\rho\kappa\right)+\sum_{n=1}^{\infty}A_n\frac{f_n}{g_n}\cos\frac{n\pi}{\beta}\theta=\left(1+\frac{v_0}{\delta}\right)\cos\theta-1, \qquad \text{for} \quad 0\le|\theta|\le\alpha, \tag{2.9}$$

where

$$\frac{A_0}{2}=a_0\frac{1-\rho^2}{\rho^2}, \qquad A_n = a_n\, g_n, \quad \text{for } n\ge1, \tag{2.10}$$

and

$$\begin{aligned}
g_n &= (n\pi-\beta)\frac{\rho^2\beta^2\left(\rho^{2n\pi/\beta}-1\right)^2-\left(\rho^2-1\right)^2 n^2\pi^2\rho^{2n\pi/\beta}}{\left[\rho^2\beta\left(\rho^{2n\pi/\beta}-1\right)+n\pi\left(\rho^2-1\right)\right]\beta^2\rho^{2+n\pi/\beta}},\\
f_n &= \frac{2n^2\pi^2\left(\rho^2-1\right)\left(\kappa\rho^2+1\right)\rho^{2n\pi/\beta}-(\kappa-1)\rho^2\beta^2\left(\rho^{2n\pi/\beta}-1\right)^2+n\pi(\kappa+1)\rho^2\beta\left(\rho^{4n\pi/\beta}-1\right)}{(\beta+n\pi)\left[\rho^2\beta\left(\rho^{2n\pi/\beta}-1\right)+n\pi\left(\rho^2-1\right)\right]\rho^{1+n\pi/\beta}}.
\end{aligned} \tag{2.11}$$

To remove the rigid body displacement v_0, we apply the operator $(D + D^{-1})$ on equation (2.9) as suggested in [16, 17], where

$$D\phi=\frac{d\phi}{d\theta}, \qquad D^{-1}\phi=\int_0^{\theta}\phi(s)\,ds, \tag{2.12}$$

thus obtaining

$$\left[\frac{A_0}{2}\frac{\rho^2}{1-\rho^2}\left(\frac{2}{\rho}-\rho+\rho\kappa\right)+1\right]\theta-\sum_{n=1}^{\infty}A_n\frac{f_n}{g_n}\left(\frac{\beta}{n\pi}-\frac{n\pi}{\beta}\right)\sin\frac{n\pi}{\beta}\theta, \qquad \text{for} \quad 0\le|\theta|\le\alpha, \tag{2.13}$$

Then, we apply the procedure used in [18] for solving a set of dual series equations similar to eqns

(2.8) and (2.13). To this aim, we rearrange equations (2.8) and (2.13) in the form

$$\frac{A_0}{2}+\sum_{n=1}^{\infty}A_n\cos nt=0,\qquad \text{for}\quad \alpha'\le|t|\le\pi, \tag{2.14}$$

$$\sum_{n=1}^{\infty}A_n\sin nt=(c\,A_0+d)\,t+\sum_{n=1}^{\infty}h_n\,A_n\sin nt,\qquad \text{for}\quad 0\le|t|\le\alpha', \tag{2.15}$$

where $t=\pi\theta/\beta$, $\alpha'=\pi\alpha/\beta$, and

$$\begin{aligned} c&=\frac{2+\rho^2(\kappa-1)}{(1+\kappa)(1-\rho^2)}\,\frac{\beta}{2\pi},\\ d&=\frac{\beta}{(1+\kappa)\,\pi\rho},\\ h_n&=1-\frac{f_n}{(1+\kappa)\,\rho\,g_n}\left(\frac{\beta}{n\pi}-\frac{n\pi}{\beta}\right), \end{aligned} \tag{2.16}$$

being

$$\lim_{n\to\infty}n\,h_n=\frac{\beta}{\pi}\frac{1-\kappa}{1+\kappa}. \tag{2.17}$$

The set of dual equations and (2.14) and (2.15) can now be solved by using the procedure proposed in [19] and adopted also in [18], based on the introduction of an auxiliary stress function φ such that

$$\frac{A_0}{2}+\sum_{n=1}^{\infty}A_n\cos nt=H(\alpha'-t)\cos\frac{nt}{2}\int_0^{\alpha'}\frac{\varphi(s)}{\sqrt{\cos nt-\cos n\,s}}\,\mathrm{d}s,\qquad \text{for}\quad 0\le|t|\le\pi, \tag{2.18}$$

where H denotes the unit step function. Then, the coefficients A_n of the Fourier cosine series expansion (2.18), for $n\ge 0$, are given in [18, 22]:

$$A_0=\sqrt{2}\int_0^{\alpha'}\varphi(s)\,\mathrm{d}s, \tag{2.19}$$

$$A_n=\frac{1}{\sqrt{2}}\int_0^{\alpha'}[P_n(\cos s)+P_{n-1}(\cos s)]\,\varphi(s)\,\mathrm{d}s,\qquad \text{for}\quad n\ge 1, \tag{2.20}$$

where P_n denotes the Legendre polynomials of order n [23, 24]. Now, using the following result ([25], eqn 2.6.31)

$$\frac{1}{\sqrt{2}}\sum_{n=1}^{\infty}[P_n(\cos s)+P_{n-1}(\cos s)]\sin nt=\frac{H(t-s)\cos(t/2)}{\sqrt{\cos s-\cos t}}, \tag{2.21}$$

one has from eqn (2.15) and (2.20)

$$\int_0^t\frac{\varphi(s)\,\mathrm{d}s}{\sqrt{\cos s-\cos t}}=\frac{1}{\cos(t/2)}\left[(c\,A_0+d)\,t+\sum_{n=1}^{\infty}h_n\,A_n\sin nt\right],\qquad \text{for}\quad 0\le|t|\le\alpha'. \tag{2.22}$$

The integral equation of the Abel type (2.22) can be inverted to obtain the auxiliary stress function φ, namely

$$\varphi(s)=\frac{2}{\pi}\frac{\mathrm{d}}{\mathrm{d}s}\int_0^s\frac{\sin(t/2)}{\sqrt{\cos t-\cos s}}\left[(c\,A_0+d)\,t+\sum_{n=1}^{\infty}h_n\,A_n\sin nt\right]\mathrm{d}t, \tag{2.23}$$

Using the results provided in Appendix B of [15], the integrals in eqn (2.23) can be calculated in closed form, thus obtaining

$$\varphi(s)=\frac{1}{\sqrt{2}}\left\{2(c\,A_0+d)+\sum_{n=1}^{\infty}n\,h_n\,A_n\,[P_n(\cos s)+P_{n-1}(\cos s)]\right\}\tan\frac{s}{2}. \tag{2.24}$$

The introduction of eqn (2.24) in (2.19) and (2.20) then gives the following relations for the coefficients A_n, for $n = 0, 1, 2,\ldots$:

$$A_0=-4(c\,A_0+d)\ln\left(\cos\frac{\alpha'}{2}\right)+\sum_{n=1}^{\infty}n\,h_n\,A_n\,J_n, \tag{2.25}$$

$$A_n=(c\,A_0+d)\,J_n+\frac{1}{2}\sum_{m=1}^{\infty}m\,K_{nm}\,h_m\,A_m,\qquad \text{for}\quad n\geq 1, \tag{2.26}$$

where

$$J_n=\int_0^{\alpha'}[P_n(\cos s)+P_{n-1}(\cos s)]\tan\frac{s}{2}\,\mathrm{d}s=\frac{1}{n}[P_{n-1}(\cos\alpha')-P_n(\cos\alpha')], \tag{2.27}$$

$$\begin{aligned}K_{nm}&=\int_0^{\alpha'}[P_n(\cos s)+P_{n-1}(\cos s)][P_m(\cos s)+P_{m-1}(\cos s)]\tan\frac{s}{2}\,\mathrm{d}s\\&=\frac{(1+\cos\alpha')\sin^2\alpha'}{2(n^2-m^2)}[(n+1)P_{m-1}^{(0,1)}(\cos\alpha')P_{n-2}^{(1,2)}(\cos\alpha')-(m+1)P_{n-1}^{(0,1)}(\cos\alpha')P_{m-2}^{(1,2)}(\cos\alpha')],\end{aligned} \tag{2.28}$$

and $P_n^{(a,b)}(t)$ denotes the Jacobi polynomials and

$$\lim_{n\to\infty}J_n=0. \tag{2.29}$$

The results provided in Section 3 in [26] have been used in calculating the integrals (2.27) and (2.28) together with eqn (3.3) reported in [27]. A detailed derivation of the result (2.28) is illustrated in Appendix B. Note that for $n = m$ the coefficient K_{nn} in (2.28) must be calculated as a limit.

Finally, the total load P acting on the pin must be equal to the resultant of the contact pressure distribution, namely

$$P=-2\,r_i\int_0^{\alpha}\sigma_{rr}(r_i,\theta)\cos\theta\,\mathrm{d}\theta\,. \tag{2.30}$$

By using eqn $(2.4)_1$, one gets

$$P=8\mu\,\delta\,\rho\int_0^{\alpha}\left(\frac{A_0}{2}+\sum_{n=1}^{\infty}A_n\cos\frac{n\pi\theta}{\beta}\right)\cos\theta\,\mathrm{d}\theta, \tag{2.31}$$

namely

$$P=8\mu\,\delta\,\rho\left[\frac{A_0}{2}\sin\alpha+\sum_{n=1}^{\infty}A_n\frac{\sin\alpha\,\cos(n\pi\theta/\beta)-(n\pi/\beta)\cos\alpha\,\sin(n\pi\theta/\beta)}{1-(n\pi/\beta)^2}\right]. \tag{2.32}$$

3. Approximate solution

To solve the non-homogeneous linear system of infinite algebraic equations (2.25) and (2.26) for the unknown coefficients A_n, for n = 0, 1, 2,…, we choose a sufficiently large integer N and rewrite eqns (2.25) and (2.26) in the truncated form:

$$A_0 = -4(c\,A_0 + d)\ln\left(\cos\frac{\alpha'}{2}\right) + \sum_{n=1}^{N} n\,h_n\,A_n\,J_n, \tag{3.1}$$

$$A_n = (c\,A_0 + d)\,J_n + \frac{1}{2}\sum_{m=1}^{N} m\,K_{nm}\,h_m\,A_m, \qquad \text{for} \quad n = 1, 2, ..., N, \tag{3.2}$$

thus obtaining a linear system of N+1 equations for the N+1 unknowns A_n, for n = 0, 1, 2,…, N. Once the linear system (3.1) and (3.2) is solved, then the solution can be refined by considering an additional number M of terms, using the approximate relations

$$A_n = (c\,A_0 + d)\,J_n + \frac{1}{2}\sum_{m=1}^{n-1} m\,K_{nm}\,h_m\,A_m, \qquad \text{for} \quad n = N+1, N+2, ..., M, \tag{3.3}$$

which exploit the behavior (2.17) and (2.29) of h_n and J_n for large n.

The relation between the applied load and the contact half-angle α in Fig. 1 is found by using an inverse method. Namely, for every assigned value of α the first N+1 coefficients of the series expansions of the stress and displacement fields (2.4) and (2.5) is calculated by solving the linear system (3.1) and (3.2), and advantageously extended to a number M+1 of term according to (3.3). Their knowledge allows to evaluate the corresponding load P defined in (2.32) which produces the assigned contact angular amplitude α.

The results presented in the next Section are obtained by considering a number of terms $N \geq 30$ in the truncated system (3.1)-(3.2) and a total number of terms $M = 2N$ in the sums for stress and displacement. Preliminary tests proved that this number of terms is suitable for obtaining sufficiently accurate results.

4. Results

To define the beam angular extent β which better simulates the actual geometry of a pin-lug connection (Fig. 2), a matching procedure with the predictions of a FEM analysis is performed by comparing the analytical results concerning the contact half-angle α to the FEM predictions for the pin-lug connection, for four different values of the aspect ratio $\rho = r_i/r_o$, also considered in previous works, namely 0.77, 0.667, 0.5 and 0.376, which generously cover the lug practically relevant geometries. Such a comparison showed that a reasonably good agreement between the analytical results and the FEM numerical predictions is attained for $\beta = 0.56\,\pi$.

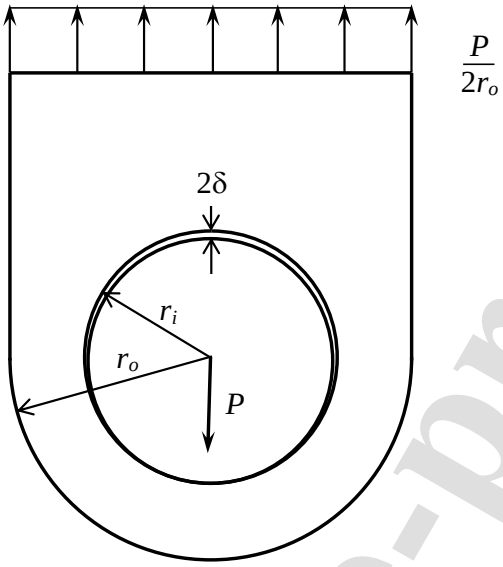

Figure 2. Geometry and loading of the pin-lug connection considered in the FEM simulations.

The normalized variations of the contact half-angle α with the loading factor Ψ used in previous works on pin-lug contact problems with clearance [10, 28], defined by

$$\Psi = \frac{3P}{8(1+\nu)\mu\delta}\left(\frac{r_o + r_i}{r_o - r_i}\right)^3, \tag{4.1}$$

have been obtained and plotted in nondimensional form in Figs. 3*a*-6*a* under plane stress loading condition for $\beta = 0.56\,\pi$ and for a Poisson coefficient $\nu = 0.3$, typical of steel. Note that the load factor Ψ accounts for the load, Young's modulus, clearance, and, although approximately, lug geometry. As the load factor is increased, the contact angular extent increases non-linearly and tends to $\pi/2$.

It can be observed that, for the considered value of β, the analytical results (solid line) fit reasonably well with the FEM predictions (dashed line) for the considered four aspect ratios of the curved beam (lug), see Figs. 3*a*-6*a*. A small improvement would be achieved by making the angle β slightly depend on the aspect ratio ρ, but this occurrence is not taken into consideration here for the sake of conciseness.

As the pin load increases, and so the loading factor Ψ defined in (4.1), the contact angular extent between the pin and the beam also increases non-linearly. In particular, for a very thin lug, namely for ρ approaching 1, the contact half-angle α tends to $\pi/2$ as the loading factor Ψ becomes very large. For a thick lug instead, the contact half-angle α tends to an extent moderately smaller than

$\pi/2$ as the loading factor Ψ increases, in agreement with the result provided in [19], where a theoretical maximum contact half-angle around 84°, namely 0.467 π, is found for a circular inclusion in an infinite elastic medium. As a general rule, for a very high pin-load that causes a contact angular extent close to the maximum asymptotic value, the size of the contact region increases very slowly with the load, until an increase in load produces an almost linear increase in the contact pressure, namely the response of the beam becomes almost linear within this range.

Note that the contact half-angle α depends on the aspect ratio ρ, as well as on the ratio $P/(E\delta)$ appearing in the definition (4.1) of Ψ, where $E = 2(1+\nu)\mu$ is the Young modulus of the beam material, and thus it does not depend on P, E and δ separately.

The normalized distributions of the contact pressure along the contact zone $p(\theta) = -\sigma_{rr}(r_i, \theta)$ are also plotted in Figs. 3*b*-6*b*. There it can be observed that the distribution of the contact pressure is almost Hertzian when the loading level is low enough (black lines), as observed in [8] and more recently in [9]. However, the pressure changes significantly as the loading magnitude increases, since two pressure peaks (bumps) take place just before the contact end points, where the pressure tends to vanish. In this case, the contact pressure is almost uniform in the central part of the contact region, in agreement with the predictions of the 1D beam model of the pin-lug connection proposed by the authors in the preliminary work [28]. There, a uniform pressure distribution is found along the whole contact region, except at the lift off points, where a point force is introduced according to the 1D beam solution for an elastic open ring fitted on a rigid cylinder provided in [14]. The contact angular extent predicted by the 1D beam model adopted in [28] turns out to be underestimated apparently due to the assumptions of transversal inextensibility of the classical beam theory as well as to the point force model applied at the contact end, which simulates the pressure bump observed in the present study but does not allow for pressure distribution. The 2D elastic model adopted here corrects these shortcomings at the cost of a greater analytical complexity.

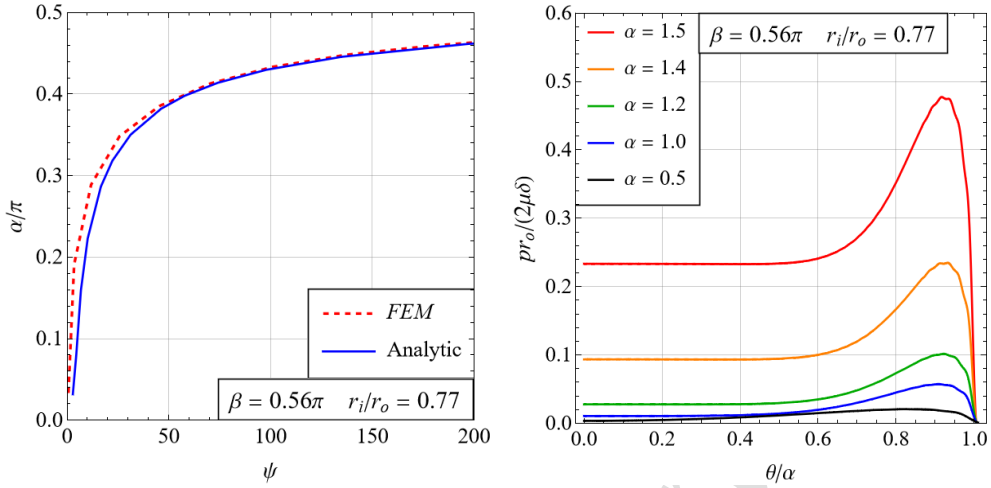

(*a*) (*b*)

Figure 3. Normalized variations of the contact half-angle α with the loading factor ψ provided by the present analytical formulation and by FEM (*a*), and of the contact pressure *p* with the angular coordinate θ (*b*). Both plots refer to the angular extent of the beam β = 0.56π and to the aspect ratio r_i/r_o = 0.77.

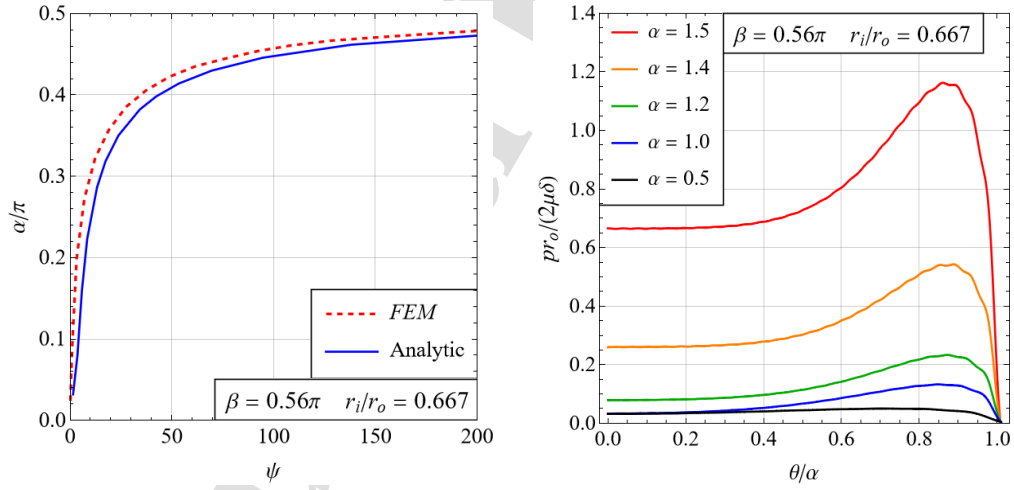

(*a*) (*b*)

Figure 4. Normalized variations of the contact half-angle α with the loading factor ψ provided by the present analytical formulation and by FEM (*a*), and of the contact pressure *p* with the angular coordinate θ (*b*). Both plots refer to the angular extent of the beam β = 0.56π and to the aspect ratio r_i/r_o = 0.667.

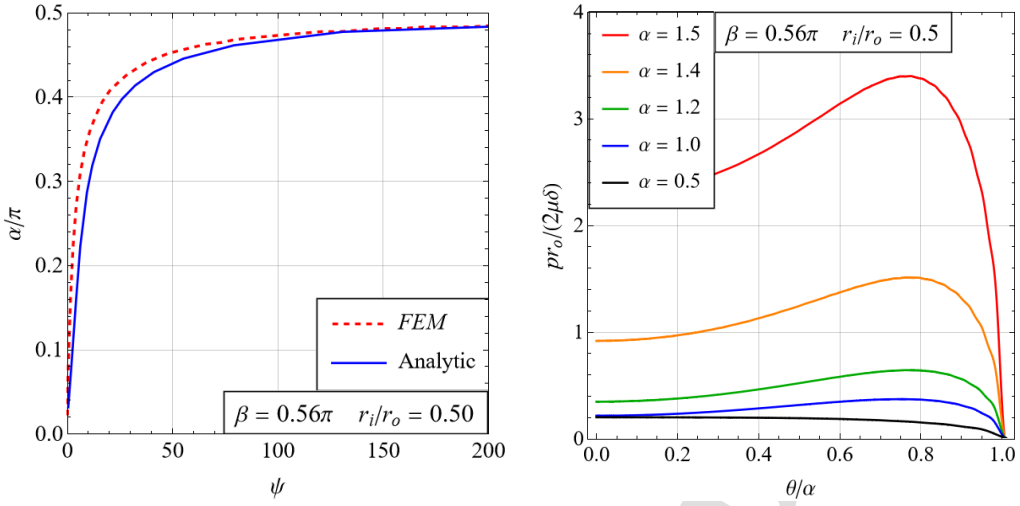

(*a*) (*b*)

Figure 5. Normalized variations of the contact half-angle α with the loading factor ψ provided by the present analytical formulation and by FEM (*a*), and of the contact pressure *p* with the angular coordinate θ (*b*). Both plots refer to the angular extent of the beam β = 0.56π and to the aspect ratio r_i/r_o = 0.50.

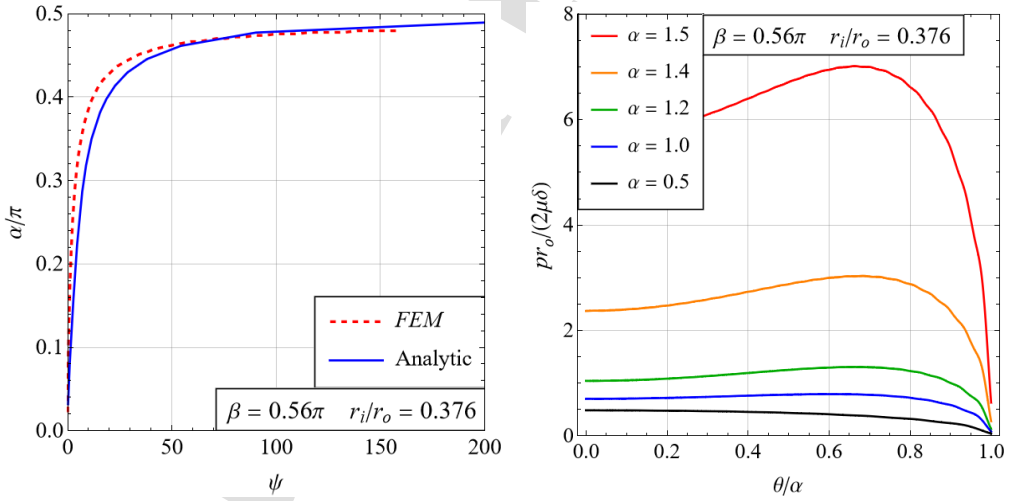

(*a*) (*b*)

Figure 6. Normalized variations of the contact half-angle α with the loading factor ψ provided by the present analytical formulation and by FEM (*a*), and of the contact pressure *p* with the angular coordinate θ (*b*). Both plots refer to the angular extent of the beam β = 0.56π and to the aspect ratio r_i/r_o = 0.376.

The distributions of the contact pressure for the limiting cases of a very thin beam (ρ = 0.95) and a very thick beam (ρ = 0.95) are plotted in Figs. 7*a* and 7*b*, respectively. These results show that the location and the width of the contact pressure peak varies with the aspect ratio of the beam. Indeed, for a very thin beam, the pressure distribution displays a sharp peak just before the ends of the contact zone and is almost constant inside the contact zone (Fig. 7*a*), in agreement with the predictions of the 1D beam model proposed in [28], where the contact pressure peak is modelled by a concentrated load. As the beam thickness increases, the width of the contact pressure peak also increases and its location shifts toward the center of the contact zone (see also Figs. 3*b*-6*b*). It occurs exactly there as ρ tends to vanish, namely for a very thick beam (Fig. 7*b*), thus approaching the Hertzian pressure distribution.

In Fig. 7*a*, one can observe that the contact pressure exhibits numerical oscillations near a sharp peak due to the Gibbs phenomenon. These oscillations can be easily mitigated by using Lanczos sigma factors [29], e. g. as in [30, 31].

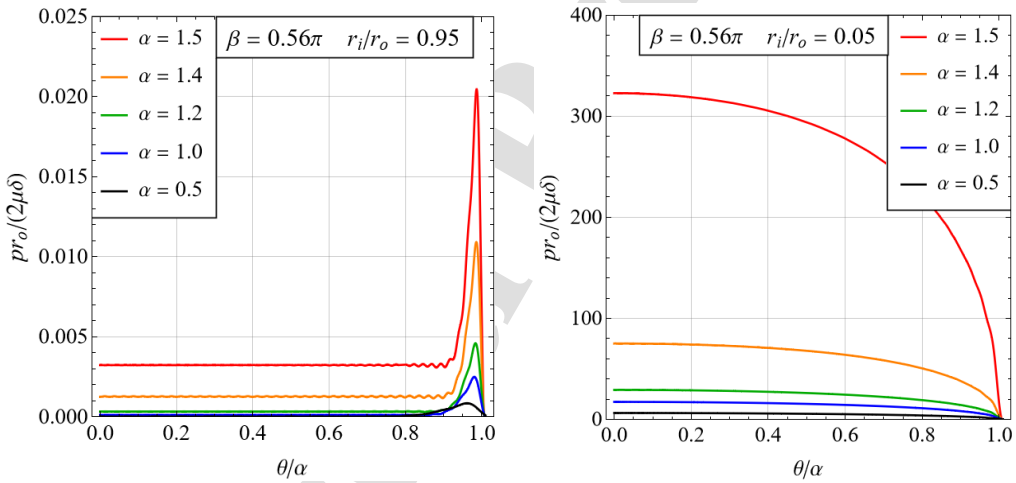

(*a*) (*b*)

Figure 7. Normalized variations of the contact pressure *p* with the angular coordinate θ for a very thin beam (*a*) and a very thick beam (*b*), for increasing values of the contact half-angle α. Both plots refer to the angular extent of the beam β = 0.56π.

The normalized variations of the hoop stress along the contact region $\sigma_{\theta\theta}(r_i, \theta)$ are plotted in Fig. 8 for the four aspect ratios considered in Figs 3-6. These results also show that the hoop stress is almost constant in the central part of the contact zone and it displays a large increase at the ends. Moreover, as the load increases, and thus the size of the contact region also increases, the hoop stress changes its sign and the location of its maximum magnitude. Indeed, for low loading level the hoop stress is compressive (negative) along the contact zone and attains its largest magnitude at the center, namely at $\theta = 0$. As the load increases, the hoop stress becomes tensile starting from the ends of the contact region ($\theta = \pm\alpha$), where it attains the maximum values within the contact zone for sufficiently large load P.

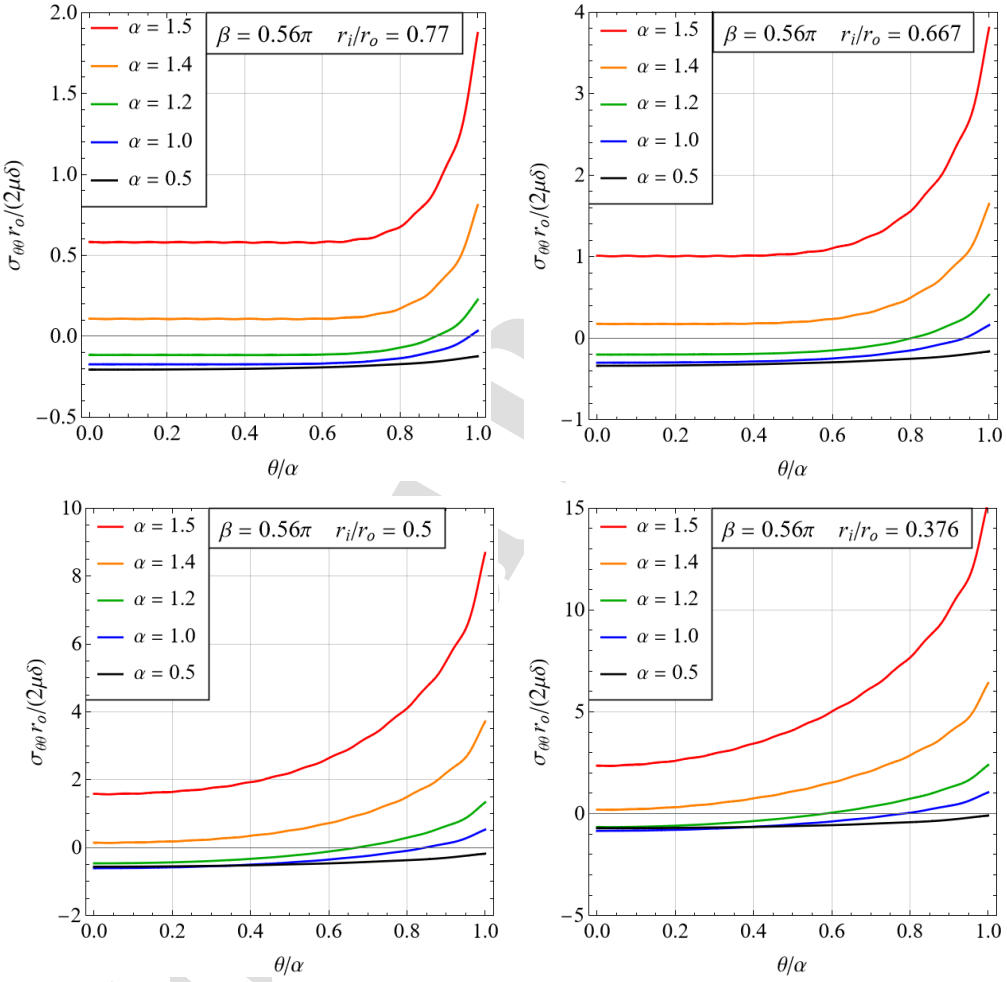

Figure 8. Normalized variations of the hoop stress $\sigma_{\theta\theta}$ along the contact region with the angular coordinate θ for the angular extent of the beam $\beta = 0.56\pi$ and for four different aspect ratios.

The normalized variations of the von Mises equivalent stress, plotted in Fig. 9, also display an almost uniform stress level at the center of the contact zone, especially for thin lugs, and a remarkable increase at the end of the contact as the load P is increased. It is interesting to note that the maximum equivalent stress is attained at the center of the contact zone for low loading level, whereas it moves to the contact end points as the load is increased. The transition occurs for a loading level causing a contact half-angle of about 1 rad, namely $\alpha \approx 0.32\ \pi$, and a bit less for thinner lugs (e. g. for the case r_i/r_o = 077). In terms of loading factor Ψ, the transition occurs for Ψ about 20, as it follows from Fig. 3*a*-7*a*, a bit more for thin lugs and a bit less for thick lugs.

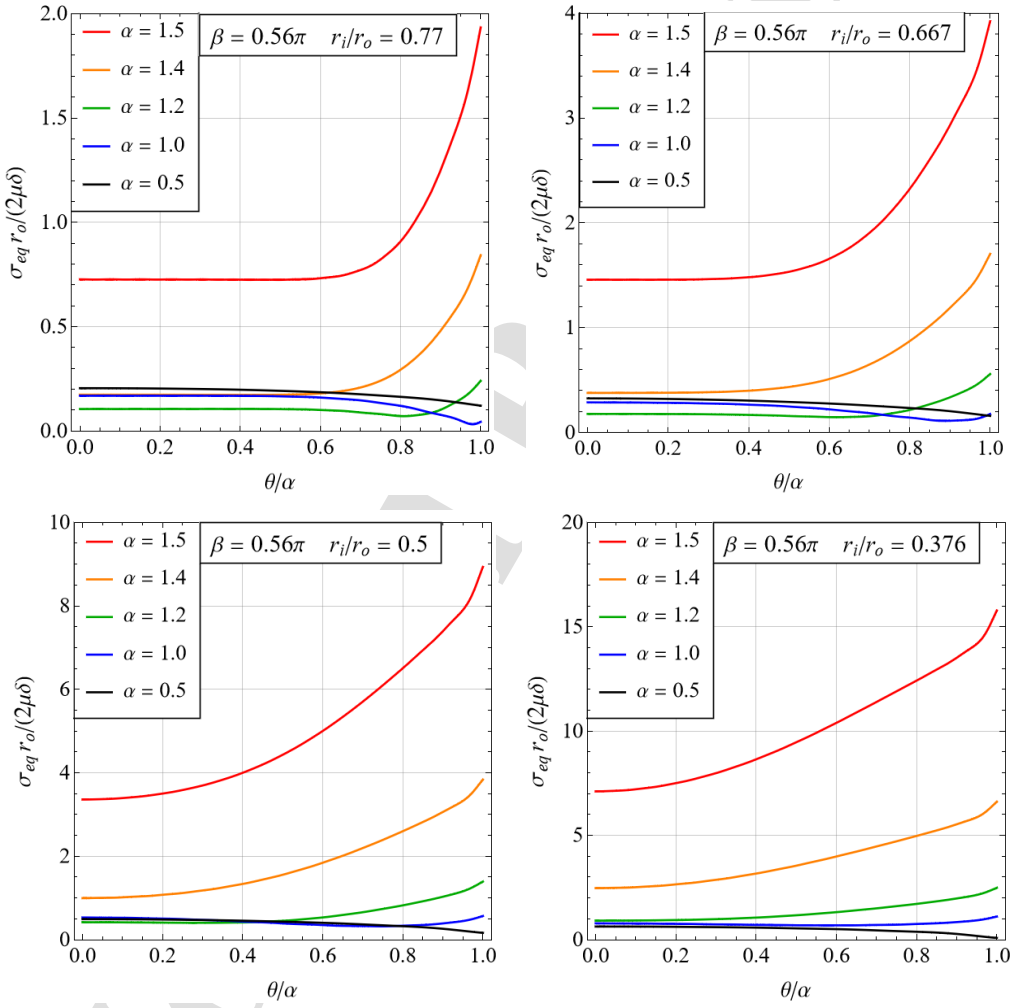

Figure 9. Normalized variations of the von Mises equivalent stress σ_{eq} along the contact region with the angular coordinate θ for the angular extent of the beam β = 0.56π and for four different aspect ratios.

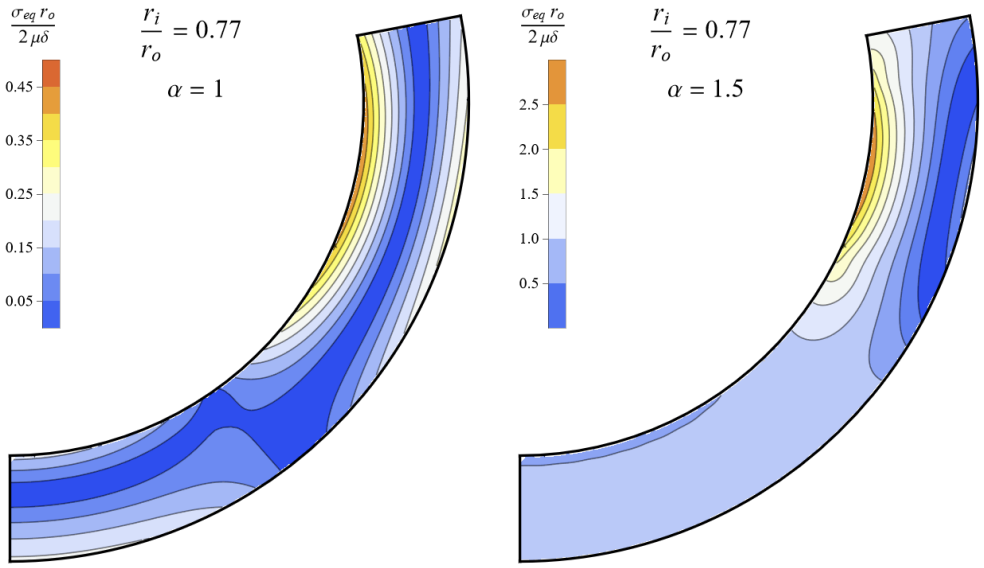

(*a*) (*b*)

Figure 10. Contour plots of the normalized von Mises equivalent stress σ_{eq} within a thin curved beam with aspect ratio $\rho = 0.77$, for $\alpha = 1$ (*a*) and $\alpha = 1.5$ (*b*). The angular extent of the beam is $\beta = 0.56\pi$.

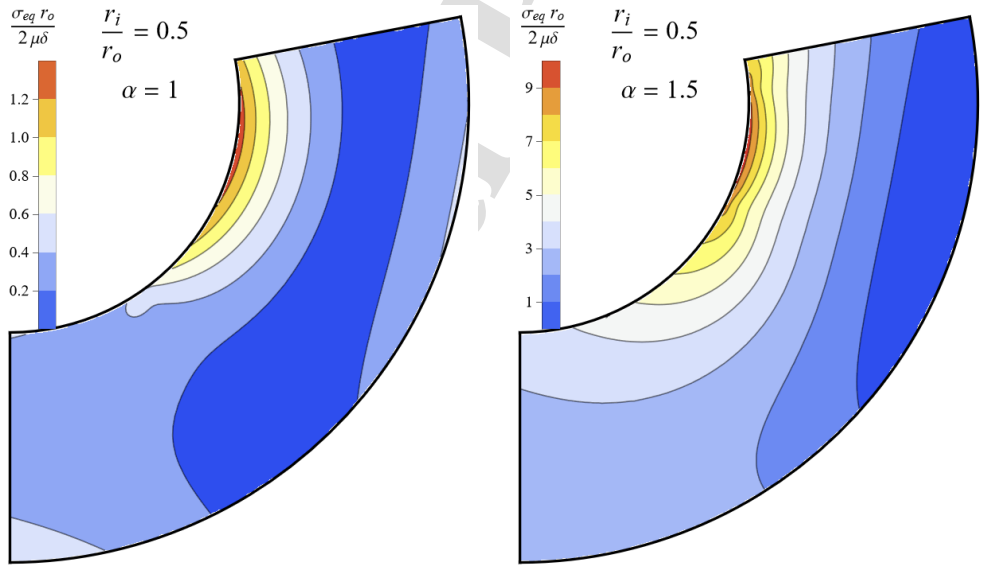

(*a*) (*b*)

Figure 11. Contour plots of the normalized von Mises equivalent stress σ_{eq} within a thick curved beam with aspect ratio $\rho = 0.5$, for $\alpha = 1$ (*a*) and $\alpha = 1.5$ (*b*). The angular extent of the beam is $\beta = 0.56\pi$,

The contour plots of the normalized von Mises equivalent stress σ_{eq} within a thin and a thick curved beam with an angular extent of 0.56π provided by the present 2D analytical approach are plotted in Figs. 10 and 11, respectively, for two different values of the contact angular extent, namely $\alpha = 1$ and $\alpha = 1.5$. Due to the symmetry, only the right-side region ($\theta \geq 0$) of the curved beam is represented. Obviously, both the load P and the stress level remarkably increase with the extent of the contact zone α. These plots show that the maximum von Mises equivalent stress is attained on the upper surface of the beam, out of the contact region, at an angular coordinate θ of about 73° independent of the loading and geometry, in agreement with the findings in [32, 33] for the hoop stress.

The results retrieved in this paper in terms of stresses are more realistic than those achieved by describing the lug in term of a curved, purely flexural 1D beam [28]. In fact, the presence of an unrealistic concentrated contact force in the 1D beam-like model precludes the possibility of deriving reliable stresses. The 2D analytical model favoured in this paper corrects the above shortcome, since the contact pressure produces a bump of finite magnitude. Therefore, an interesting extension of this paper would be to examine whether the approach of [11] proposing an interpretation of the above concentrated force in terms of a Hertzian-type distribution describing the pressure bump, correctly modifies the unrealistic concentrated force of the 1D curved beam model into a more realistic pressure bump of finite maximum value, according to the results obtained here by using the 2D theory of elasticity.

Conclusions

An analytical 2D solution for the stress and displacement fields in an elastic circular beam indented by a rigid circular pin with clearance in frictionless contact with the upper inner surface of the beam is derived herein by using a modified Fourier-Michell solution and solving a set of dual series equations. The angular extent of the circular beam is chosen to best fit with the FEM predictions for a pin-lug connection. The progressive character of the contact in the presence of an initial clearance between the pin and the lug is discussed in detail. In particular, the contact region increases non-linearly with the load factor and approaches an asymptotic value close to $\pi/2$ as the load becomes very large. The pressure distributions along the contact zone are plotted for various aspect ratios and load factors. They show that the Hertzian distribution is valid only for very low load levels and small contact zone, while for high loading levels the central pressure remains reasonably constant, and two pressure bumps take place near the ends of the contact zone. The advantages of the proposed 2D modelling of the lug are clearly underlined with respect to the 1D counterpart. Finally,

the employment of a load factor in the dimensioning of the pin-lug connection may support the designer efficiently. All these results are of practical relevance in the design of pin-lug connections.

Acknowledgements

Financial support within the framework of the grant MIUR-PRIN2020 "Mathematics for industry 4.0" (code 2020F3NCPX) is gratefully acknowledged.

References

[1] A. Persson 1964. On the stress distribution of cylindrical elastic bodies in contact. PhD. Dissertation Chalmers University, Sweden.

[2] A.K. Rao, 1978. Elastic analysis of pin joints. Comp. Struct. 9, 125-144.

[3] M. Ciavarella, P. Decuzzi, 2001. The state of stress induced by the plane frictionless cylindrical contact. I. The case of elastic similarity. Int. J. Solids Struct. 38(26-27), 4507-4523.

[4] M. Ciavarella, P. Decuzzi, 2001. The state of stress induced by the plane frictionless cylindrical contact. II. The general case (elastic dissimilarity). Int. J. Solids Struct. 38(26-27), 4525-4533.

[5] N. Sundaram, T.N. Farris, 2010a. Mechanics of advancing pin-loaded contacts with friction. J. Mech. Phys. Solids 58(11), 1819-1833.

[6] N. Sundaram, T.N. Farris, 2010b. The generalized advancing conformal contact problem with friction, pin loads and remote loading–case of rigid pin. Int. J. Solids Struct. 47(6), 801-815.

[7] T.S. Ramamurthy, 1989. New studies on the effect of bearing loads in lugs with clearance fit pins. Compos. Struct. 11(2), 135-150.

[8] G.S. Wang, 1994. Stress analysis for a lug under various conditions. J. Strain Anal. Eng. Des. 29(1), 7-16.

[9] Y. Li, R. Huang, S. Zhao, J. Wang, 2022. Contact pressure analysis of pin-loaded lug with clearance. Adv. Mech. Eng. 14(6), 16878132221107475.

[10] A. Strozzi, M. Giacopini, E. Bertocchi, S. Mantovani, A. Baldini, 2022. Towards an analytical model of a pin-lug connection. Int. J. Solids Struct. 253, 111446.

[11] J.R. Barber, 2018. Contact mechanics. Springer International Publishing, Berlin.

[12] A. Strozzi, A. Baldini, M. Giacopini, S. Rivasi, R. Rosi, 2007. Maximum stresses in a taper-shanked round-ended lug loaded by an oblique concentrated force. Strain 43(2), 109-118.

[13] A. Strozzi, A. Baldini, M. Nascimbeni, 2006. Maximum equivalent stress in a pin-loaded lug subject to inclined loading. J. Strain Anal. Eng. Des. 41(4), 297-309.

[14] V.I. Feodosiev, 2005. Advanced stress and stability analysis: Worked examples. Springer Science & Business Media, Berlin.

[15] B. Noble, M.A. Hussain, 1969. Exact solution of certain dual series for indentation and inclusion problems. Int. J. Eng. Sci. 7(11), 1149-1161.

[16] T. Omar, H.A. Hassan, 1991. Approximate solution for an indentation problem using dual series equations. Int. J. Eng. Sci. 29(2), 187-194.

[17] H.A.Z. Hassan, 1997. Concentrated force acting on an elastic inclusion in a thick-walled tube. J. Eng. Math. 32, 73-86.

[18] J.M. Block, L.M. Keer, 2007. Partial contact of an elastic coated cylinder pressed by a rigid flat surface. J. Tribol. 129(1), 60-64.

[19] J.P Hou, D.A. Hills, 2001. Contact between a pin and a plate with a hole under interference-fit and clearance-fit conditions. Proc. Inst. Mech. Eng. Part C: J. Mech. Eng. Sci. 215(6), 629-639.

[20] C.S. Liu, K. Zhang, R. Yang, 2007. The FEM analysis and approximate model for cylindrical joints with clearances. Mech. Mach. Theory 42(2), 183-197.

[21] J.R. Barber, 2010. Elasticity. Springer, Dordrecht.

[22] J. Dundurs, K.C. Tsai, L.M. Keer, 1973. Contact between elastic bodies with wavy surfaces. J. Elast. 3, 109-115.

[23] A. Strozzi, 2012. A note on the Legendre series solution of the biharmonic equation for cylindrical problems. J. Elasticity, 108(1), 119-123.

[24] A. Strozzi, E. Bertocchi, 2015. A note on the Legendre series solution of the Laplace equation for cylindrical problems. J. Elasticity, 118(1), 109-112.

[25] I.N. Sneddon, 1966. Mixed boundary value problems in potential theory. John Wiley, New York.

[26] B. Noble, J.R. Whiteman, 1970. Solution of dual trigonometric series using orthogonality relations. SIAM J. Appl. Math. 18(2), 372-379.

[27] M. Derevyagin, N. Juricic, 2020. An asymptotic formula for integrals of products of Jacobi polynomials. J. Stoch. Anal. 1(4), 8.

[28] A. Strozzi, E. Radi, 2022. Analytical tool assisting the designer of pin-lug connections. Struct. Submitted.

[29] C. Lanczos, 1956. Applied Analysis. Prentice Hall, Englewood Cliffs.

[30] S.L. Crouch, S.G. Mogilevskaya, 2006. Loosening of elastic inclusions. Int. J. Solids Struct. 43(6), 1638-1668.

[31] G. Singh, T.K. Bhandakkar, 2019. Simplified approach to solution of mixed boundary value problems on homogeneous circular domain in elasticity. ASME J. Appl. Mech. 86(2), 021007.

[32] R.J. Grant, J. Smart, P. Stanley, 1994. A parametric study of the elastic stress distribution in pin-loaded lugs. J. Strain Anal. Eng. Des. 29(4), 299-307.

[33] R.J. Grant, B.C.D. Flipo, 2009. Parametric study of the elastic stress distribution in pin-loaded lugs modelled in two and three dimensions and loaded in tension. J. Strain Anal. Eng. Des. 44(6), 473-489.

Appendix A. Michell solution in polar coordinates

According to the Michell solution, the Airy stress function for a plane problem of linear elasticity in polar coordinates (r, θ), which is even in the coordinate θ, assumes the general form [18]:

$$\phi = \frac{2\mu\delta}{r_o}\left[a_0 r^2 + b_0 \ln r + \sum_{n=1}^{\infty} (a_n r^{n\pi/\beta} + b_n r^{2+n\pi/\beta} + c_n r^{-n\pi/\beta} + d_n r^{2-n\pi/\beta}) \cos\frac{n\pi\theta}{\beta} \right],$$

where the exponent of the radial coordinate inside the sum are not integers. Then, the function ϕ satisfies the biharmonic equation $\nabla^4\phi = 0$ for every arbitrary parameter β and arbitrary coefficients a_0, b_0, a_n, b_n, c_n, d_n. Moreover, the corresponding stress field (2.4) follows from the relations [21, 31]:

$$\sigma_{rr} = \frac{1}{r}\frac{\partial\phi}{\partial r} + \frac{1}{r^2}\frac{\partial^2\phi}{\partial\theta^2}, \qquad \sigma_{\theta\theta} = \frac{\partial^2\phi}{\partial r^2}, \qquad \sigma_{r\theta} = -\frac{\partial}{\partial r}\left(\frac{1}{r}\frac{\partial\phi}{\partial\theta}\right),$$

Then, the corresponding displacement field (2.5) is derived as illustrated in [21].

Appendix B. Integral involving Legendre and Jacobi polynomials

To calculate the integral (2.28) we need the following relation provided in [26]:

$$P_n(t) + P_{n-1}(t) = (1+t)P_{n-1}^{(0,1)}(t), \qquad \text{for} \quad n \geq 0,$$

and the following result proved in [27] in eqn (3.3):

$$\int_x^1 (1+t)P_{n-1}^{(0,1)}(t)P_{m-1}^{(0,1)}(t)\,\mathrm{d}t = \frac{(1+x)(1-x^2)}{2(n^2-m^2)}[(n+1)P_{m-1}^{(0,1)}(x)P_{n-2}^{(1,2)}(x) - (m+1)P_{n-1}^{(0,1)}(x)P_{m-2}^{(1,2)}(x)].$$

Then

$$\begin{aligned} K_{nm} &= \int_0^{\alpha'} [P_n(\cos s) + P_{n-1}(\cos s)][P_m(\cos s) + P_{m-1}(\cos s)]\tan\frac{s}{2}\,\mathrm{d}s = \\ &= \int_{\cos\alpha'}^1 [P_n(t) + P_{n-1}(t)][P_m(t) + P_{m-1}(t)]\frac{\mathrm{d}t}{1+t} = \\ &= \int_{\cos\alpha'}^1 (1+t)\,P_{n-1}^{(0,1)}(t)\,P_{m-1}^{(0,1)}(t)\,\mathrm{d}t = \\ &= \frac{(1+\cos\alpha')\sin^2\alpha'}{2(n^2-m^2)}[(n+1)P_{m-1}^{(0,1)}(\cos\alpha')P_{n-2}^{(1,2)}(\cos\alpha') - (m+1)P_{n-1}^{(0,1)}(\cos\alpha')P_{m-2}^{(1,2)}(\cos\alpha')], \end{aligned}$$

for $n \neq m$. By taking the limit for $m \to n$ one gets

$$K_{nn}=\frac{(1+\cos\alpha')\sin^2\alpha'}{4n}\left\{P_{n-1}^{(0,1)}(\cos\alpha')P_{n-2}^{(1,2)}(\cos\alpha')+(n+1)\times\right.$$
$$\left.\left[P_{n-1}^{(0,1)}(\cos\alpha')\frac{d}{dn}P_{n-2}^{(1,2)}(\cos\alpha')-P_{n-2}^{(1,2)}(\cos\alpha')\frac{d}{dn}P_{n-1}^{(0,1)}(\cos\alpha')\right]\right\}.$$

Declaration of interests

☒ The authors declare that they have no known competing financial interests or personal relationships that could have appeared to influence the work reported in this paper.

☐ The authors declare the following financial interests/personal relationships which may be considered as potential competing interests: